Inelastic neutron scattering study of magnetic excitations in the kagome antiferromagnet potassium jarosite

2006 J. Phys.: Condens. Matter 18 8847

(http://iopscience.iop.org/0953-8984/18/39/015)

INSTITUTE OF PHYSICS PUBLISHING JOURNAL OF PHYSICS: CONDENSED MATTER

J. Phys.: Condens. Matter **18** (2006) 8847–8858 doi:10.1088/0953-8984/18/39/015

Inelastic neutron scattering study of magnetic excitations in the kagome antiferromagnet potassium jarosite

F C Coomer[1,2], A Harrison[1,2,3,8], G S Oakley[1,2], J Kulda[3], J R Stewart[3], J A Stride[3,9], B Fåk[4], J W Taylor[5] and D Visser[5,6,7]

[1] School of Chemistry and EaStChem, The University of Edinburgh, The King's Buildings, West Mains Road, Edinburgh EH9 3JJ, UK
[2] The Centre for Science at Extreme Conditions, Erskine Williamson Building, The University of Edinburgh, The King's Buildings, Mayfield Road, Edinburgh EH9 3JZ, UK
[3] Institut Laue-Langevin, BP 156, 38042 Grenoble Cedex, France
[4] Département de Recherche Fondamentale sur la Matière Condensée, SPSMS, CEA Grenoble, 38054 Grenoble, France
[5] The ISIS Facility, Rutherford Appleton Laboratory, Chilton, Didcot, Oxon OX11 0QR, UK
[6] Department of Physics, University of Warwick, Coventry CV4 7AL, UK
[7] IRI, TU Delft, Mekelweg 15, 2629 JB Delft, The Netherlands

E-mail: a.harrison@ed.ac.uk

Received 16 May 2006, in final form 31 July 2006
Published 15 September 2006
Online at stacks.iop.org/JPhysCM/18/8847

Abstract

We report an inelastic neutron scattering study of coherent magnetic excitations in powder and single-crystal samples of the model kagome antiferromagnet potassium iron jarosite, $KFe_3(OH)_6(SO_4)_2$. Initial measurements on a natural single crystal using a triple-axis spectrometer revealed a mode with a zone-centre gap of 7 meV that showed little dispersion within the kagome layers, as well as some indication of a mode with a zone-boundary energy of approximately 20 meV. However, the high background from hydrogen in the sample made it very difficult to search for other excitations. In the absence of suitable deuterated crystals, measurements were performed on deuterated powders using time-of-flight neutron spectrometers over a range of temperatures that include $T_N \cong 64$ K. This confirmed the flat 7 meV mode as well as dispersive modes that reached to higher energies. The origin of these modes is discussed in relation to the most likely Hamiltonian for the magnetic degrees of freedom in this material, and estimates are made of the strength of the nearest-neighbour exchange, J_1, and contributions from a Dzyaloshinsky–Moriya interaction or single-ion anisotropy arising from a crystal field.

[8] Author to whom any correspondence should be addressed.
[9] Present address: School of Chemistry, University of New South Wales, Sydney 2052, Australia.

1. Introduction

The design, synthesis and study of frustrated antiferromagnets has remained at the forefront of research in solid-state physics for almost two decades [1–4], driven by the challenges and insights they provide in many-body phenomena, and also by potential applications. One system that possesses a relatively simple Hamiltonian but potentially complex physics is the nearest-neighbour Heisenberg antiferromagnet on a kagome lattice (HKAFM). For classical spins, the ground state is degenerate, and two of the possible choices of ground state—the so-called $q = 0$ and $\sqrt{3} \times \sqrt{3}$ spin structures—are shown in figure 1.

Perturbations to the Hamiltonian such as further-neighbour interactions may select a particular ground state [5–11], while quantum fluctuations, which are expected to be significant for small spins, may lead to spin-liquid states [12–17]. Whilst there is a substantial body of theoretical work on the HKAFM [5, 18–28], suitable model systems for experimental work are much more limited [2, 29–32]. The most widely studied system to date has been based on the jarosite family of minerals, with general chemical formula $AM_3(SO_4)_2(OH)_6$ [6, 7, 10, 11, 33–46]; here A is a univalent cation, and for magnetic members of the family, the trivalent metal ion M is most commonly iron. Such studies have established that all the iron compounds possess strong antiferromagnetic exchange, with Weiss temperatures of the order of -800 K from susceptibility measurements. Almost all members of the family show long-range magnetic order below a temperature of approximately 50 K, and the type of order is believed to reflect the nature of additional perturbations to the simple near-neighbour exchange, including further-neighbour exchange, crystal-field terms [11] and Dzyaloshinsky–Moriya interactions [8, 9]. Co-operative effects in this family of compounds are also sensitive to structural and magnetic inhomogeneities [38, 47, 48], and this is believed to play a role in the somewhat different behaviour of the hydronium ($A = D_3O^+$) member of the family [35, 37]: it has been postulated [45] that hydronium iron jarosite has random fluctuations in the near-neighbour exchange as a consequence of random protonation of the oxygen atoms in the exchange pathways, and this leads to glassy magnetic behaviour at low temperature [49]. This experimental work has stimulated considerable complementary theoretical studies of perturbed kagome systems, revealing rich phase diagrams. In order to test the theory, and ensure that it relates qualititatively and quantitatively to real materials, it is necessary to have accurate and precise values for the terms in the Hamiltonian, and the most direct way to do this is through measurement of spin-wave dispersion by inelastic neutron scattering. This in turn poses considerable challenges in preparing suitable samples: it is difficult to make chemically pure compounds, and also to produce single crystals greater than a few microns across. However, in the past few years both these challenges have been overcome [43, 45, 50], though the optimum size of crystal synthesis to date has been at the limit of what the most incisive probe of magnetic fluctuations—inelastic neutron scattering—can be applied to. An alternative source of crystalline samples is the Earth [51], and natural jarosite crystals have been found with volumes of the order of 10 mm^3.

Here we report inelastic neutron scattering studies of the magnetic excitations in such a natural crystal of $KFe_3(SO_4)_2(OH)_6$ (which is the most common natural jarosite, and the one for which there is the greatest choice of suitable crystals), using a triple-axis spectrometer to map the dynamic susceptibility, $\chi''(\mathbf{Q}, \omega)$, at particular values of wavevector $\mathbf{Q}$, and $\omega = \Delta E/\hbar$, where ΔE is the neutron energy transfer, by scanning along either of these variables. Whilst this technique allows very detailed characterization of excitations, it is less well suited to surveys of $(\mathbf{Q}, \omega)$ space when the system is poorly characterized, or $\chi''(\mathbf{Q}, \omega)$ is small. An alternative method is to use time-of-flight (TOF) techniques, in conjunction with multi-detectors, to map a large range of $\mathbf{Q}$ and ω. Here we report such a study, conducted on

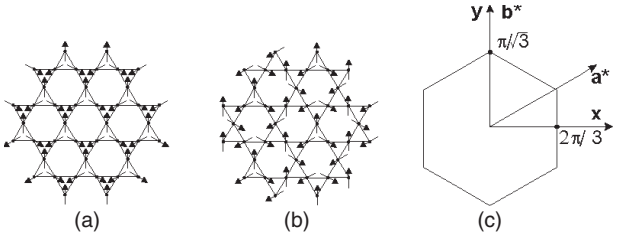

Figure 1. The kagome lattice, with (a) the $q = 0$ array, (b) the $\sqrt{3} \times \sqrt{3}$ spin configuration, and (c) the reciprocal lattice vectors and extent of the first Brillouin zone for the purely two-dimensional real-lattice cell of edge a together with the definition of the co-ordinate axes **x** and **y**.

powders of $KFe_3(SO_4)_2(OD)_6$. We also discuss the interpretation of the data in the light of the most likely leading terms in the Hamiltonian beyond the nearest-neighbour exchange and show that the parameters that we determine are consistent with those derived from thermodynamic data such as the magnetic susceptibility, and the observed spin structures.

2. Experimental details

2.1. Sample composition and magnetization studies

The natural sample of jarosite that was used originated in Eureka, Utah, USA and had a mass of 14.9 mg, corresponding to a volume of approximately 4.9 mm^3, calculated using a density of $\rho = 3 \times 10$ g cm^{-1} [51]. Some of the surface was facetted in a manner that was compatible with the $R\bar{3}m$ space group, and the orientation of the c-axis was inferred from this; this orientation was later confirmed by neutron diffraction. The atomic composition was checked by energy-dispersive x-ray emission using a Hitachi S4700 instrument fitted with an Oxford ISIS EDS system. This revealed the presence of potassium (but no other element that was also likely to sit on the A site) and iron (but no other element such as aluminium that was also likely to sit on the M site); sulfur and oxygen were also detected. A very precise and accurate determination of the site coverage with respect to iron was not possible using these energy-dispersive x-ray emission measurements, our estimate being $95 \pm 3\%$ coverage. It was also studied by neutron diffraction, yielding the occupancy of the iron site to be $96 \pm 1\%$. A rocking scan, performed by rotating the crystal about an axis perpendicular to a horizontal scattering plane for the magnetic 1 0 5/2 reflection at 20 K, revealed two crystallites, separated by approximately 0.5°. dc magnetization measurements were performed on the aligned crystal using a superconducting quantum interference detector (SQUID) magnetometer, together with polarized neutron diffraction measurements in zero magnetic field, and the results of these studies are reported elsewhere [52]. However, it should be noted here that the Néel temperatures determined from susceptibility and neutron diffraction measurements were 64.0(5) and 63.00(5) K respectively, the cell parameters at 20 K were determined as $a = b = 7.230(4)$ Å and $c = 17.13(1)$ Å, and the magnetic propagation vector was determined to be 0 0 3/2. A deuterated powder sample was also prepared, using standard techniques [38].

2.2. Neutron spectroscopy

The single-crystal sample was mounted inside a helium-flow cryostat on the triple-axis spectrometer IN8 at the Institut Laue–Langevin (ILL) in one of two orientations. In the first, the vectors $\mathbf{a}^*$ and $\mathbf{b}^*$ were in the horizontal scattering plane, and in the second the vectors $(\mathbf{a}^* + \mathbf{b}^*)$ and $\mathbf{c}^*$ were in that plane. The monochromator (vertically focusing) and analyser

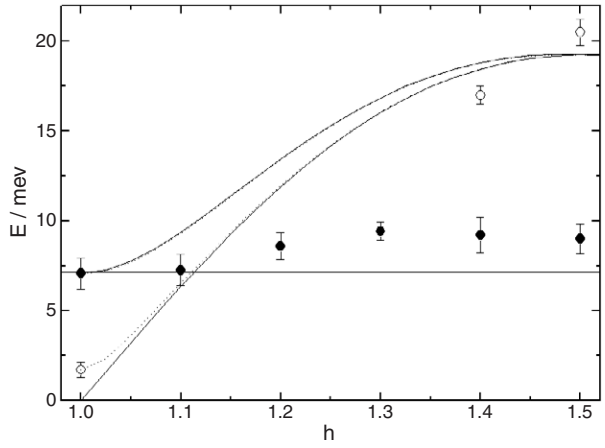

Figure 2. Dispersion of excitations observed in a natural single crystal of potassium iron jarosite for neutron energy loss up to 24 meV along $\mathbf{Q} = (h\ h\ 1.5)$ at 5 K. Solid circles distinguish excitations attributed to the weakly dispersive mode, while open circles distinguish excitations attributed to the more strongly dispersive modes. The dotted lines represents spin-wave branches calculated for the crystal field (CF) model with parameters J_1, E, and D optimized to fit the strongly dispersing data at $\mathbf{Q} = (1.0\ 1.0\ 1.5)$, $(1.4\ 1.4\ 1.5)$, $(1.5\ 1.5\ 1.5)$, as well as the weakly dispersive mode at $(1.0\ 1.0\ 1.5)$; the solid lines represent the spin-wave branches calculated using the Dzyaloshinsky–Moriya (DM) model with parameters J_1 and D_z optimized through fits to the same set of excitations. The two upper branches calculated using the DM model partly or wholly obscure branches calculated using the CF model.

(horizontally focusing) both used the 0 0 2 reflection of pyrolytic graphite, and there was 60′ collimation between the monochromator and the sample, with other parts of the instrument open. The instrument was run with a fixed, final wavevector such that $|\mathbf{k}_f| = 2.66$ Å^{-1}. A search for magnetic excitations was made at 5 K, first with a constant energy transfer of 3 meV, and then constant-**Q** scans were carried out over a range of neutron energy transfer from -2 to 25 meV. Scans were concentrated near prominent magnetic Bragg peaks such as 1 1 3/2.

For measurements on the powder sample, approximately 10 g of the material was loaded in an aluminium can and inserted in a helium cryostat, and placed on either the TOF spectrometer MARI at the ISIS Facility, UK, or IN4 at the ILL. Incident energies of 8, 15 and 60 meV were used on MARI, allowing us to resolve excitations down to 1 meV from the elastic scattering, while on IN4 the incident energy was 48 meV, allowing excitations to be resolved from the elastic scattering down to approximately 4 meV.

3. Results

3.1. Excitations in the single-crystal sample

Constant-**Q** data taken from (1 1 1.5) to (1.5 1.5 1.5), over the energy range 0–24 meV showed a sharp excitation with a modest dispersion, ranging from approximately 7–9 meV in energy. This was least-squares fitted to a Gaussian curve convoluted with the instrumental resolution function to yield the energies summarized in figure 2. In addition, and prompted by the observation of a more strongly dispersive mode in a powder sample (see below, section 3.2), we looked for excitations of smaller scattering cross-section that lay on a branch whose energy reached approximately 20 meV at the zone boundary. The most distinct examples of these additional excitations are also given in figure 2, while data taken at points $(h\ h\ 1.5)$ with h

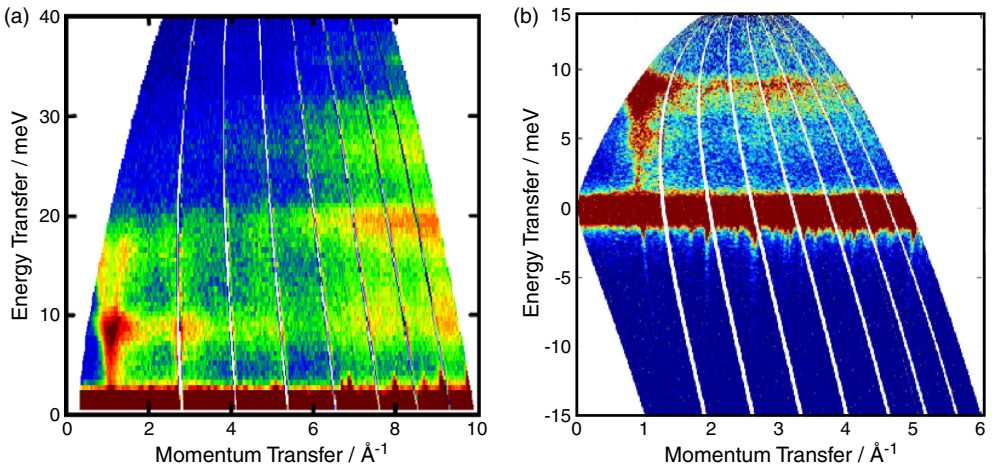

Figure 3. (a) $\chi''(\mathbf{Q}, \omega)$ for deuterated potassium iron jarosite powder measured on spectrometer MARI at 5 K with incident energies 60 meV and (b) $S(\mathbf{Q}, \omega)$ measured for the same sample on the same instrument with an incident energy of 15 meV.

in the range 1–1.3 could not be distinguished from the background and/or the less strongly dispersing excitation.

3.2. Excitations in the powder sample

The imaginary part of the dynamic susceptibility of the system, $\chi''(\mathbf{Q}, \omega)$, was calculated from the dynamic structure factor, $S(\mathbf{Q}, \omega)$, using the detailed balance condition:

$$\chi''(\mathbf{Q}, \omega) = (1 - \exp(-\hbar\omega/k_B T)) \cdot S(\mathbf{Q}, \omega). \tag{1}$$

Plots of $\chi''(\mathbf{Q}, \omega)$ or $S(\mathbf{Q}, \omega)$ taken from data gathered on spectrometer MARI at 5 K, and then on spectrometer IN4 over a range of temperatures that include T_N, are displayed in figures 3 and 4. The weakly dispersive mode at ∼7 meV that was observed in the single-crystal sample is also apparent in the TOF data, and disappears on warming through T_N (figures 4 and 5). The intensity of the mode is modulated in Q, with clear maxima in the regions of $|\mathbf{Q}| = 1$, and 3 Å^{-1}. The MARI data also reveal dispersive modes rising from a point centred near $|\mathbf{Q}| = 1$ Å^{-1} (see figure 3(a)) and stretching towards an energy compatible with that observed at the zone boundary energy in the single-crystal measurements. Above 10 meV, one clearly sees the two branches corresponding to $\boldsymbol{\tau} \pm \mathbf{q}$ (figure 3(a)). This dispersive mode has an energy gap at the magnetic zone centre of 1.7 ± 0.4 meV.

If one assumes coupling between the kagome layers to be negligible, we need only consider the symmetry of the problem in the ab planes and the real lattice vectors are then $\mathbf{a} = a\mathbf{x}$ and $\mathbf{b} = -(a/2)\mathbf{x} + (\sqrt{3}a/2)\mathbf{y}$, where $a = 7.23$ Å is the edge of the real lattice in the $q = 0$ structure (equal in potassium iron jarosite to twice the nearest-neighbour iron–iron separation), and orthogonal vectors $\mathbf{x}$ and $\mathbf{y}$ are displayed in figure 1(c). The reciprocal lattice then has vectors $\mathbf{a}^*/2\pi = (1/a)\mathbf{x} + (1/\sqrt{3}a)\mathbf{y}$ and $\mathbf{b}^*/2\pi = (2/\sqrt{3}a)\mathbf{y}$, which for potassium iron jarosite leads to a second Brillouin zone centred at $|\mathbf{Q}| = 4\pi/\sqrt{3}a = 1.00$ Å^{-1}— compatible with the observed position of the first intensity maximum in the TOF data.

In principle, one could model such data to obtain leading parameters in the magnetic Hamiltonian if an expression for $S(\mathbf{Q}, \omega)$ was available and a powder average taken; in the

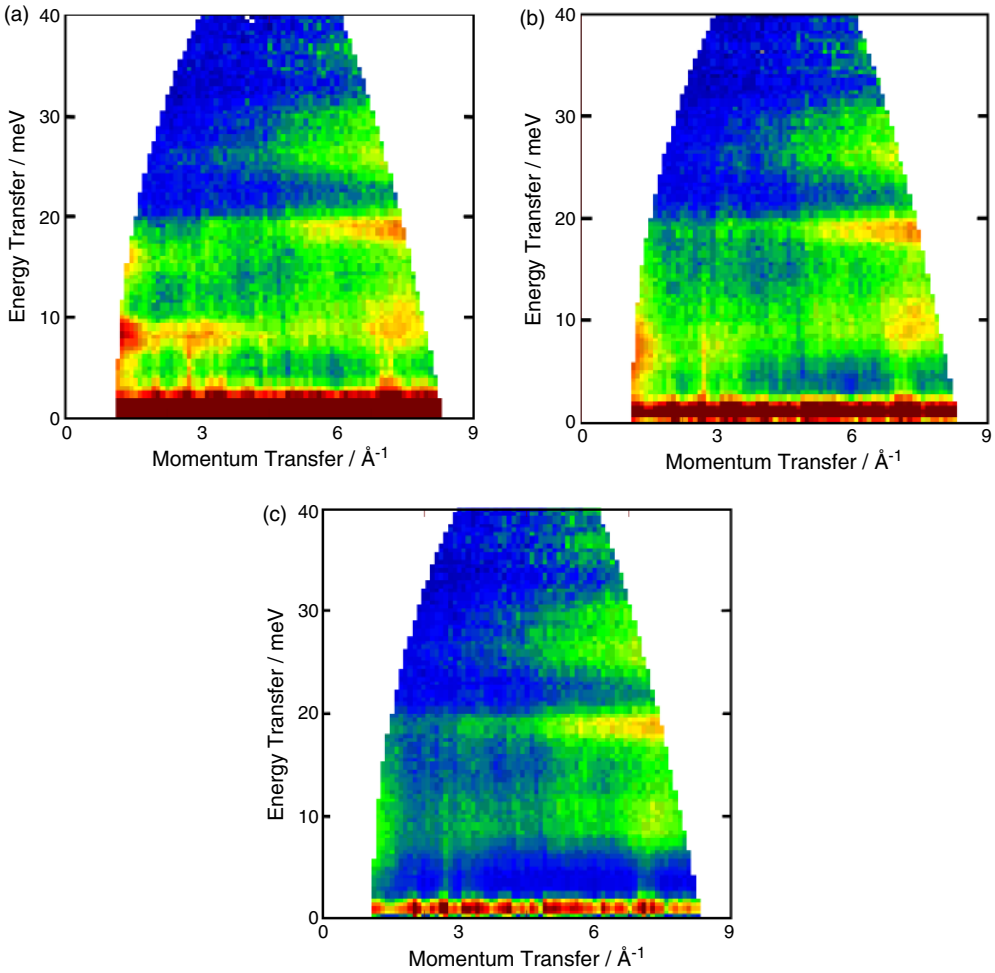

Figure 4. $\chi''(\mathbf{Q}, \omega)$ for deuterated potassium iron jarosite powder ($T_N \cong 64$ K) measured on spectrometer IN4 at (a) 1.5 K, (b) 57.5 K and (c) 150 K.

absence of such an expression, it is unreliable to assume that some of the more distinct dispersive elements correspond to specific modes.

A second feature may also be distinguished at low temperature at approximately twice the energy of the weakly dispersive mode, with a similarly flat dependence on **Q**, though it is also broader in energy and less intense. This is most likely to reflect the zone-boundary energy of the one-magnon excitation spectrum, though it could also be some form of two-magnon excitation. Figure 5 displays cuts through the data along an energy axis, centred at $|\mathbf{Q}| = 1.75$ Å^{-1}, as a function of temperature, clearly revealing a mode centred near 8 meV, and the broader feature centred near 16 meV.

4. Discussion

4.1. General considerations on the Hamiltonian

Expressions already exist for the dispersion of spin-waves in various forms of kagome antiferromagnet, so we first discuss which, if any, are appropriate for this system. The

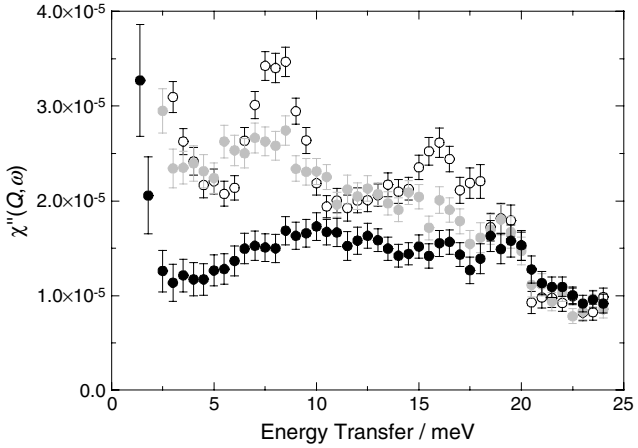

Figure 5. $\chi''(\mathbf{Q}, \omega)$ for deuterated potassium iron jarosite ($T_N \cong 64$ K) measured on spectrometer IN4 at $Q = 1.75$ Å^{-1} and temperatures 1.5 K (open circles), 57.5 K (grey circles) and 150 K (closed circles).

leading term is undoubtedly the nearest-neighbour exchange, J_1, which alone would lead to the following Hamiltonian:

$$H = J_1 \sum_{\langle i,j \rangle} \mathbf{S}_i \cdot \mathbf{S}_j \tag{2}$$

where the sum is over all spins i and their nearest-neighbours j. This term gives three branches in the Brillouin zone for the $q = 0$ structure: one is a non-dispersive, zero-energy mode (ε_1), and the other two (ε_2, ε_3) are degenerate, and disperse to a maximum energy $2JS$ at the zone boundary [5, 53].

Consideration both of the various exchange pathways and also of the collective properties of the iron jarosites has led to the conclusion that inter-plane exchange, J', is much less than J_1 [50]; further-neighbour in-plane exchange interactions J_2 and J_3 are likely to be intermediate between J_1 and J'. Dispersion relations have been derived for antiferromagnets with up to third further-neighbour interactions within the kagome layers [5, 53]. Other perturbations to the simple Hamiltonian (2) that have been considered are single-ion anisotropies arising from crystal field (CF) terms [11] and a Dzyaloshinsky–Moriya (DM) interaction [8, 9]. Both these terms raise the energy of the non-dispersive, zero-energy mode, and may also perturb the energy of the dispersive modes [54].

4.2. Single-ion anisotropy and the crystal field model

Crystal-field effects are anticipated to be weak for the octahedrally coordinated high-spin $3d^5$ ion Fe^{3+}. However, the deviation of the local coordination from perfect cubic symmetry, combined with finite spin–orbit coupling, leads to additional single-ion anisotropy terms of the following form appearing in the Hamiltonian [11]:

$$H = D \sum_i (S_i^{z'})^2 - E \sum_i (S_i^{x'})^2 - (S_i^{y'})^2 \tag{3}$$

where x', y' and z' refer to a local coordinate system in which z' is the four-fold axis of the axially distorted coordination octahedron of iron, and x' and y' are perpendicular to z' and each

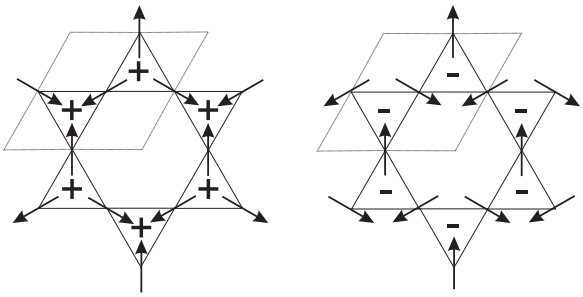

Figure 6. Different forms of the $q = 0$ spin structures of the kagome lattice in the jarosite structure. The rhombus depicts the nuclear unit cell projected onto the ab plane with the b-axis horizontal, while (a) and (b) possess a uniform chirality $+1$ and -1, respectively.

other and bisect the angle O–Fe–O for those atoms in the equatorial plane of the canted FeO_6 octahedra. Dispersion relations have been derived for this case [11] as follows:

$$\varepsilon_i(\mathbf{q}) = S\sqrt{(J_1(2-\lambda_i(\mathbf{q})) + 2(E-D) + 2(E+D)(\cos^2\theta))(2J_1(1+\lambda_i(\mathbf{q})) + 2(E+D)(2\cos^2\theta - 1))} \tag{4}$$

where θ is the canting of the four-fold axis of the distorted FeO_6 octahedra from the crystallographic c-axis, and the values of $\lambda_i(\mathbf{q})$ are:

$$\lambda_1 = -1; \tag{5a}$$

$$\lambda_{2,3} = \frac{1}{2}\left(1 \pm \sqrt{-3 + 4\left(\cos^2 q_x + \cos^2\left(\frac{q_x - \sqrt{3}q_y}{2}\right) + \cos^2\left(\frac{q_x + \sqrt{3}q_y}{2}\right)\right)}\right) \tag{5b}$$

where q_x and q_y are components of $\mathbf{q}$ in directions $\mathbf{x}$ and $\mathbf{y}$, as defined in section 3.2 and illustrated in figure 1(c).

The zero-energy mode of the simple kagome antiferromagnet remains non-dispersive, but for $D, E \ll J_1$ now lies at the energy:

$$\varepsilon_1 = S\sqrt{6J_1(D+E)(2\cos^2\theta - 1)}. \tag{6}$$

D and E also have an influence on the most stable spin array, favouring structures in which just one type of spin chirality is found in the triangular plaquettes (for instance, selecting the $q = 0$ structure over the $\sqrt{3} \times \sqrt{3}$ spin structure), and further selecting $+1$ or -1 chirality, depending on the sign of E (figures 6(a) and (b)). Finally, competition between D, E and J_1 may lead to spin-canting, with the angle δ between the spins and the xy planes when $D, E \ll J_1$ given by [11]:

$$\sin\delta \cong \frac{D+E}{3J_1}\sin 2\theta. \tag{7}$$

Iron jarosites studied to date have a $q = 0$ spin structure of $+1$ chirality as far as the projections of moments in the ab plane are concerned, and some degree of canting towards the c-axis, depending on the temperature. When the potassium salt is cooled from the paramagnetic state, it may pass through two successive phase transitions, though this does vary between samples [6, 55, 56]. The higher-temperature phase has an 'umbrella' spin structure, with a significant component of spin along the c-axis (of the order of 10°–20°); the lower-temperature

phase has a much smaller component along the c-axis. The sense of the canting in any ab plane is antiparallel to that in nearest-neighbour planes, so in zero field there is no spontaneous moment. Magnetization measurements yield an estimate of the canted angle in the low-temperature phase to be at least 0.65(6)° at 50 K [50], and zero-field magnetic polarimetry indicates that the upper limit for any canting is of the order of 1° at 20 K [52]. This latter result was for the same sample for which the current single-crystal inelastic neutron scattering data are reported.

Excitations at $\mathbf{Q} = (1.4\ 1.4\ 1.5)$ and $(1.5\ 1.5\ 1.5)$ and the excitation of lower energy at $\mathbf{Q} = (1.0\ 1.0\ 1.5)$ were attributed to the more strongly dispersive modes ($\varepsilon_{2,3}$) and values of energy calculated in terms of J_1, D and E using $\lambda_{2,3}$ as defined in (5*b*), while the energy of the zone-centre mode at 7 meV was attributed to the weakly dispersive branch (ε_1) and its energy calculated using the value of λ_1 given in (5*a*). The value of θ was taken to be 21°, based on neutron diffraction data taken on the same sample at 20 K [52]. Values of J_1, D and E were then optimized through least-squares fitting of the appropriate expressions to the data, yielding the following values: $J_1 = 3.50(3)$ meV, $D = 0.47(2)$ meV and $E = 0.038(2)$ meV. These in turn yield an estimate of the spin canting angle $\delta = 1.86°$ from equation (7), which is significantly larger than the upper limit determined experimentally.

4.3. Dzyaloshinsky–Moriya interactions

A DM interaction introduces the following term to the Hamiltonian:

$$\sum_{\langle i,j\rangle} \mathbf{D}_{ij} \cdot \mathbf{S}_i \times \mathbf{S}_j. \tag{8}$$

Here, the vector $\mathbf{D}_{ij}$ may have components both parallel and perpendicular to the kagome layers D_{xy} and D_z, respectively; the former is forbidden by symmetry when the kagome layers of Fe ions act as a mirror plane for the nearest-neighbour oxygen atoms, and is therefore allowed in the iron jarosites with canting of the iron–oxygen octahedra away from the c-axis. Depending on the balance between D_{xy}, D_z and J_1, various forms of spin-structure may be stablilized. D_z selects one of the two types of $q = 0$ spin-array depicted in figures 6(a) and (b) with $+1$ or -1 chirality, respectively—with positive values of D_z favouring the former. D_{xy} favours the canting of moments out of the kagome layers. The canting angle η may be estimated from the values of D_{xy}, D_z and J_1 using the expression:

$$\tan(2\eta) = \frac{2D_{xy}}{\sqrt{3}J_1 + D_z} \tag{9}$$

where D_{xy} and D_z may also influence the spin-wave dispersion, and in particular D_z raises the energy of the zero-energy mode so that it becomes [9, 54]:

$$\varepsilon_1 = S\sqrt{6\sqrt{3}J_1 D_z + 18D_z^2}. \tag{10}$$

We fitted the same spin-wave excitations as were used in the analysis of the previous section with the CF model: the excitation of higher energy at $\mathbf{Q} = (1.0\ 1.0\ 1.5)$, together with the two most distinct points on what is believed to be the strongly dispersive modes, were fitted to (10) and the closest dispersion relation available in the literature for a kagome antiferromagnet with a DM term [54]:

$$\varepsilon_i(\mathbf{q}) = S\sqrt{2(J_1(1+\lambda_i(\mathbf{q})) + D_z\sqrt{3})(J_1 + D_z\sqrt{3})(2-\lambda_i(\mathbf{q}))} \tag{11}$$

where $\lambda_i(\mathbf{q})$ is as given in (5*a*), (5*b*). The presence of a term D_{xy} will produce a gap at the zone centre for the more strongly dispersing branches, but without any explicit expression to

do this, we chose not to fit the data to the lower-energy excitation at $\mathbf{Q} = (1.0\ 1.0\ 1.5)$. The result of this analysis is illustrated in figure 2, and yields the following optimized parameters: $J_1 = 3.33(5)$ meV and $D_z = 0.21(1)$ meV. There are two further caveats to this analysis: first, both DM and CF terms may co-exist and, although it has been argued that the CF terms are likely to be substantially smaller than the DM terms [8], they may still give rise to significant errors in the optimized DM parameters; second, the fact that the mode whose energy is 7 meV at (1.0 1.0 1.5) disperses indicates that further-neighbour exchange is significant.

The xy component of $\mathbf{D}$ may be estimated from the canting angle, assuming it to be the dominant factor determining this parameter. Using a value $\eta = 1^\circ$ to provide an upper limit for the sample on which our spin-wave data were taken [52], we find from (9) that the upper limit on $|D_{xy}|$ is 0.10(2) meV; note that this analysis is unable to provide the sign of D_{xy} [54].

5. Conclusions

We have observed coherent magnetic excitations in a natural single-crystal sample of the model kagome antiferromagnet potassium iron jarosite. These modes were confirmed by TOF inelastic neutron scattering from deuterated powders, and the studies were extended to include their dependence on temperature. The spin-wave spectrum contains modes that disperse strongly in the $\mathbf{a}^*\mathbf{b}^*$ plane, as well as weakly dispersive modes whose energy scale depends both on the exchange and smaller terms in the Hamiltonian such as components of a DM interaction or a single-ion anisotropy. Appropriate spin-wave dispersion relations were fitted to the most distinct excitations. A model in which the principal perturbations to the simple near-neighbour kagome antiferromagnet arose from CF effects yield the optimized parameters: $J_1 = 3.50(3)$ meV, $D = 0.47(2)$ meV and $E = 0.038(2)$ meV; these in turn yield an estimate of the spin-canting angle $\delta = 1.86^\circ$. A second model in which a DM term D_z was present yielded the parameters $J_1 = 3.33(5)$ meV and $D_z = 0.21(1)$ meV; these parameters, together with a measured upper limit on any spin-canting out of the kagome layers, provides an estimate of 0.10(2) meV for $|D_{xy}|$. It should be noted that the values of J_1 deduced from susceptibility data [5] using a series expansion based on the simplest Hamiltonian (1) was 3.9 meV [46]. Discrepancies between the parameters may reflect the absence of further-neighbour exchange in our models.

Clearly what is needed now is a deuterated crystal of sufficient size to perform further inelastic neutron scattering measurements of dispersions of the various magnon modes and their structure factors, together with theory that enables the calculation of these properties for a Hamiltonian that includes not only DM and single-ion anisotropy terms, but also further-neighbour in-plane exchange, and the presence of canting of moments out of the kagome layers. We should then have the most powerful set of tools to determine all of these parameters precisely and accurately, and determine whether classical theory is sufficient to explain the static and dynamic properties of classical kagome antiferromagnets.

Acknowledgments

We are grateful to the UK Engineering and Physical Sciences Research Council (EPSRC) for financial support, and to the Institut Laue–Langevin and the ISIS Facility for technical support. None of this work would have been possible without the generous loan of the sample from the Natural History Museum, London, facilitated by Mark Welch. Dick Visser thanks the NWO (The Netherlands) for financial support.

References

[1] Ramirez A P 1994 *Annu. Rev. Mater. Sci.* **24** 453–80
[2] Ramirez A P 2001 *Handbook of Magnetic Materials* vol 9, ed K J H Buschow (New York: New Holland) pp 423–520
[3] Greedan J E 2001 *J. Mater. Chem.* **11** 37–53
[4] Harrison A 2004 *J. Phys.: Condens. Matter* **16** S553–72
[5] Harris A B, Kallin C and Berlinsky A J 1992 *Phys. Rev.* B **45** 2899–919
[6] Inami T, Nishiyama M, Maegawa S and Oka Y 2000 *Phys. Rev.* B **61** 12181–6
[7] Inami T, Moritomo T, Nishiyama M, Maegawa S and Okumura H 2001 *Phys. Rev.* B **64** 054421
[8] Elhajal M, Canals B and Lacroix C 2002 *Phys. Rev.* B **66** 014422
[9] Ballou R, Canals B, Elhajal M, Lacroix C and Wills A S 2003 *J. Magn. Magn. Mater.* **262** 465–71
[10] Moritomo T, Nishiyama M, Maegawa S and Oka Y 2003 *J. Phys. Soc. Japan* **72** 2085
[11] Nishiyama M, Maegawa S, Inami T and Oka Y 2003 *Phys. Rev.* B **67** 224435
[12] Sindzingre P, Lecheminant P and Lhuillier C 1994 *Phys. Rev.* B **50** 3108–13
[13] Zeng C and Elser V 1995 *Phys. Rev.* B **51** 8318–24
[14] Lecheminant P, Bernu B, Lhuillier C, Pierre L and Sindzingre P 1997 *Phys. Rev.* B **56** 2521–9
[15] Waldtmann C, Everts H U, Bernu B, Lhuillier C, Sindzingre P, Lecheminant P and Pierre L 1998 *Eur. Phys. J.* B **2** 501–7
[16] Hastings M B 2001 *Phys. Rev.* B **63** 014413
[17] Syromyatnikov A V and Maleyev C V 2002 *Phys. Rev.* B **66** 132408
[18] Chandra P and Coleman P 1991 *Phys. Rev. Lett.* **66** 100
[19] Reimers J N, Berlinsky A J and Shi A C 1991 *Phys. Rev.* B **43** 865–78
[20] Chalker J T, Holdsworth P C W and Shender E F 1992 *Phys. Rev. Lett.* **68** 855
[21] Chubukov A 1992 *Phys. Rev. Lett.* **69** 832
[22] Sachdev S 1992 *Phys. Rev.* B **45** 12377
[23] Shender E F, Cherepanov V B, Holdsworth P C W and Berlinsky A J 1993 *Phys. Rev. Lett.* **70** 3812
[24] Azaria P, Hooley C, Lecheminant P, Lhuillier C and Tsvelik A M 1998 *Phys. Rev. Lett.* **81** 1694–7
[25] Moessner R and Chalker J T 1998 *Phys. Rev.* B **58** 12049–62
[26] Garanin D A and Canals B 1999 *Phys. Rev.* B **59** 443–56
[27] Yu W Q and Feng S P 1999 *Phys. Rev.* B **59** 13546–9
[28] Sindzingre P, Misguich G, Lhuillier C, Bernu B, Pierce L, Waldtmann C and Everts H U 2000 *Phys. Rev. Lett.* **84** 2953–6
[29] Ramirez A P, Espinosa G P and Cooper A S 1990 *Phys. Rev. Lett.* **64** 2070
[30] Elser V 1989 *Phys. Rev. Lett.* **62** 2405
[31] Awaga K, Okuno T, Yamaguchi A, Hasegawa M, Inabe T, Maruyama Y and Wada N 1994 *Phys. Rev.* B **49** 3975–81
[32] Rao C N R, Paul G, Choudhury A, Sampathkumaran E V, Raychaudhuri A K, Ramasesha S and Rudra I 2003 *Phys. Rev.* B **67** 134425/1-5
[33] Townsend M G, Longworth G and Roudaut E 1986 *Phys. Rev.* B **33** 4919
[34] Keren A, Kojima K, Le L P, Luke G M, Wu W D, Uemura Y J, Takano M, Dabkowska H and Gingras M J P 1996 *Phys. Rev.* B **53** 6451–4
[35] Wills A S and Harrison A 1996 *J. Chem. Soc.-Faraday Trans.* **92** 2161–6
[36] Lee S H, Broholm C, Collins M F, Heller L, Ramirez A P, Kloc C, Bucher E, Erwin R W and Lacevic N 1997 *Phys. Rev.* B **56** 8091–7
[37] Wills A S, Harrison A, Mentink S A M, Mason T E and Tun Z 1998 *Europhys. Lett.* **42** 325–30
[38] Wills A S, Harrison A, Ritter C and Smith R I 2000 *Phys. Rev.* B **61** 6156–69
[39] Wills A S 2001 *Phys. Rev.* B **6305** 4430
[40] Grohol P D and Nocera D G 2001 *Angew. Chem. Int. Edn* **40** 1519
[41] Grohol D and Nocera D G 2002 *J. Am. Chem. Soc.* **124** 2640
[42] Nishiyama M and Maegawa S 2003 *Physica* B **329–333** 1065–6
[43] Grohol D, Nocera D G and Papoutsakis D 2003 *Phys. Rev.* B **67** 064401
[44] Grohol D, Huang Q Z, Toby B H, Lynn J W, Lee Y S and Nocera D G 2003 *Phys. Rev.* B **68** 094404
[45] Nocera D G, Bartlett B M, Grohol D, Papoutsakis D and Shores M P 2004 *Chem. Eur. J.* **10** 3850–9
[46] Grohol D, Matan K, Cho J-H, Lee S-H, Lynn J W, Nocera D G and Lee Y S 2005 *Nat. Mater.* **4** 323–8
[47] Earle S A, Ramirez A P and Cava R J 1999 *Physica* B **262** 199–204
[48] Frunzke J, Hansen T, Harrison A, Lord J S, Oakley G S, Visser D and Wills A S 2001 *J. Mater. Chem.* **11** 179–85
[49] Wills A S, Dupuis V, Vincent E, Hammann J and Calemczuk R 2000 *Phys. Rev.* B **62** R9264–7

[50] Bartlett B M and Nocera D G 2005 *J. Am. Chem. Soc.* **127** 8985–93
[51] Gaines R V, Skinner H C W, Foord E E, Mason B and Rosenzweig A 1997 *Dana's New Minerology* 8th edn (New York: Wiley)
[52] Harrison A, Oakley G S, Pettigrew K G, de Vries M, McIntrye G J, LeLièvre-Berna E, Harris M, Visser D and Wills A S 2006 in preparation
[53] Asakawa H and Suzuki M 1994 *Physica* A **205** 687–701
[54] Elhajal M 2002 Proprietes de basse energie et anisotropies d'interactions de systemes magnetiques geometriquement frustres *PhD Thesis* Grenoble 1
[55] Maegawa S, Nishiyama M, Tanaka N, Oyamada A and Takano M 1996 *J. Phys. Soc. Japan* **65** 2776–8
[56] Frunzke J, Hansen T, Harrison A, Lord J S, Oakley G S, Visser D and Wills A S 2001 *J. Mater. Chem.* **11** 179–85